https://doi.org/10.3311/PPci.42689



**Periodica Polytechnica Civil Engineering**, 70(1), pp. 189–206, 2026

# Seismic Resilience Analysis of Steel Moment Frames Equipped with Dissipative Replaceable Devices

Mohammad Amin Beheshti Masalegoo[1], Panam Zarfam[1*], Pasha Javadi[1]

[1] Department of Civil Engineering, Science and Research Branch, Islamic Azad University, 1477893855 Tehran, P.O.B. 14515/775, Iran
[*] Corresponding author, e-mail: zarfam@iau.ac.ir

Received: 31 October 2025, Accepted: 30 January 2026, Published online: 17 February 2026

**Abstract**

This study aims to probabilistically evaluate the seismic resilience of steel structures equipped with dissipative and replaceable components. These elements are specifically designed to enhance the repairability of the structures, thereby minimizing downtime and facilitating rapid post-earthquake recovery. Moreover, the effects of dissipative replaceable devices on fragility and vulnerability estimates are investigated. This study examined two steel buildings, a 6-story and a 12-story structure, considered under two distinct configurations: conventional moment-resisting frames and frames equipped with dissipative replaceable links. Preliminary designs were first developed, followed by the creation of detailed nonlinear models in OpenSees. The seismic performance was then assessed through Incremental Dynamic Analysis using a set of generic ground motion records. For each damage state, distinct recovery functions are defined, and 500 realizations are generated through the Latin Hypercube sampling technique to construct probabilistic resilience curves. The results demonstrate that incorporating dissipative replaceable devices significantly enhances the seismic performance and resilience of steel structures. Compared to conventional frames, link-equipped frames exhibited reduced inter-story drifts, leading to lower non-structural damage and concentration of inelastic demands in replaceable links rather than primary members. Fragility analysis confirmed a reduction in the probability of damage states, particularly at life safety and collapse prevention levels. Resilience indices further highlighted the superior functionality retention and faster recovery of frames with replaceable links, especially under strong earthquakes. Comparative assessment of 6- and 12-story buildings indicated that the benefits of dissipative links are consistent across different heights, with even greater improvements observed in taller structures.

**Keywords**

seismic resilience, steel structures, dissipating devices, replaceable connections, seismic fragility

## 1 Introduction

Over recent decades, seismic engineering has achieved significant progress in protecting human lives, particularly in densely populated areas. However, minimizing damage to structural and non-structural components after major earthquakes remains a critical and unresolved issue, one with serious social, economic, and environmental implications. Recent seismic events have caused widespread damage to various types of structures, including steel buildings, often compromising their functionality or even necessitating demolition and reconstruction [1–3].

To address the ongoing challenges in seismic design, particularly the need to minimize structural damage and facilitate rapid post-earthquake recovery, numerous innovative strategies have emerged, with energy dissipation systems at the forefront. Among these, passive control devices stand out for their practicality and cost-effectiveness. Their design approach involves assigning specific zones within a structure to absorb and dissipate seismic energy, often by reducing local stiffness to decouple these zones from the main structural system. This targeted energy dissipation helps protect the primary structural elements from damage.

In structural and seismic engineering, energy-dissipating elements (commonly referred to as structural fuses) play a vital role in enhancing structural performance during dynamic events. These fuses are designed to deform inelastically under seismic loads, absorbing energy that would otherwise be transmitted to the main frame. A structure equipped with such devices can typically be divided into two components: the main structural frame,

**Cite this article as:** Beheshti Masalegoo, M. A., Zarfam, P., Javadi, P. "Seismic Resilience Analysis of Steel Moment Frames Equipped with Dissipative Replaceable Devices", Periodica Polytechnica Civil Engineering, 70(1), pp. 189–206, 2026. https://doi.org/10.3311/PPci.42689

which remains elastic, and the structural fuse, which acts as a sacrificial, energy-dissipating component. Fuses can be either replaceable or non-replaceable. Replaceable fuses are engineered to be easily substituted after they reach their deformation limits, thereby enabling a faster and more economical recovery process [4, 5]. In contrast, non-replaceable fuses often require extensive repairs or complete component replacement following a damaging event. Consequently, for a structure to be considered resilient, the use of replaceable fuses is essential.

In the context of steel and composite structures, innovations such as replaceable components and self-centering systems have shown great promise in improving seismic resilience and contributing to sustainable recovery strategies [1]. Despite extensive research efforts over the past few decades [6–11], the widespread adoption of these technologies in engineering practice remains limited due to the absence of standardized design guidelines. Moreover, experimental investigations have mostly been restricted to the component level, primarily due to budget constraints, limited testing facilities, and equipment availability, highlighting the need for further system-level research and development. In this context, the RFCS DISSIPABLE project [12] was launched with the objective of experimentally investigating Dissipative and Replaceable Components (DRCs) at the structural frame level, with a particular focus on understanding their interaction with the non-replaceable parts of the system. The project combined numerical simulations and experimental testing to evaluate the seismic performance of innovative structural systems equipped with three types of DRCs, each functioning as a fuse during an earthquake [1]:

1. dissipative replaceable bracing connection;
2. dissipative replaceable link frame;
3. dissipative replaceable beam splices.

These solutions aim to enhance structural resilience by localizing damage to easily replaceable components while preserving the integrity of the main structural system.

The Dissipative Replaceable Link Frame (DRLF) system is an innovative lateral load-resisting system for steel structures. It consists of two rigid columns connected by beams with reduced beam sections (RBS) at their ends. In the current study, DRLF in the form of a flexural link is employed as a practical solution for enhancing seismic performance of steel frame. The link is strategically designed to yield under flexural demands, protecting the main frame from damage while allowing for straightforward replacement after a major event [12].

Prior to the occurrence of natural or human-induced hazards, it is essential to conduct both qualitative and quantitative assessments of the vulnerability of structures and lifeline systems [13]. In civil engineering, one of the emerging areas of focus is resilience. Quantifying resilience can provide valuable insights for decision-making processes aimed at enhancing community safety. The importance of disaster management and the identification of system or community weaknesses in the face of future hazards are key motivations for addressing resilience in this study. In recent decades, structural design and evaluation have shifted from strength-based methods to performance-based approaches. Performance-based design emphasizes estimating potential losses, including repair costs, casualties, and overall risk reduction. Its core components consist of seismic hazard assessment, seismic response analysis, failure analysis, and damage analysis. However, a major limitation of this method is the lack of attention to the recovery phase of structures or infrastructure. Hence, there is a pressing need for a framework that also incorporates the recovery process, including the role of individuals and organizations involved. Recently, resilience-based design frameworks have been developed [14–18]. These frameworks focus not only on damage and its consequences but also on the recovery process, ensuring that system functionality is sustained with minimal disruption. Section 2 elaborates on the concept and definition of resilience and introduces a framework for quantitatively evaluating the resilience of a system.

Resilience has been widely used as a performance indicator for many civil infrastructures such as hospitals, water supply networks, power grids, and transportation systems [13]. The term "resilience" originates from the Latin word *resilio*, meaning "to jump back" or "to return" [19]. In technical literature, it has been employed across various fields such as ecology, physics, psychology, and engineering, leading to a wide range of definitions (see the study by Bruneau et al. [15] for common definitions across different disciplines). Across all these domains, the common principle is the ability to return and recover from external pressures and threats – an attribute that has become a primary objective in earthquake-resistant structural design. In civil engineering, the concept of resilience is generally applied to structural components, entire structures, and critical infrastructures. Bruneau et al. [15], followed by Cimellaro et al. [16], Cimellaro et al. [20], Cimellaro et al. [21], provided a useful definition of resilience: it is a function that represents the ability of a building, bridge, lifeline,

or community to maintain performance over a given period of time, referred to as the "control time", which is usually defined by the community or stakeholders.

In recent studies, several frameworks for quantifying resilience have been proposed. One of the earliest works in this area was by Bruneau et al. [15], who introduced four dimensions of resilience: technical, organizational, social, and economic. For each dimension, they identified four key properties: robustness, redundancy, resourcefulness, and rapidity. Later, Cimellaro et al. [20] proposed an analytical framework for quantifying resilience based on dimensionless functions related to variations in functionality over a specified period, accounting for both disaster-induced damage and the recovery process. Damage was determined using system fragility functions defined through multivariate performance thresholds, incorporating uncertainties. They applied this approach to a hospital in California, considering both direct and indirect losses [22]. However, their study focused only on the technical dimension of resilience, leaving aside social and organizational aspects.

Berman and Bruneau [23] investigated the effect of seismic retrofitting on the recoverability of structures. They argued that strengthening a structure before a specific event is equivalent to shifting its fragility curve to the left, meaning that after retrofitting, a more severe event is required to produce the same level of structural damage. Consequently, retrofitted structures exhibit higher performance and are more capable of returning to their original functionality following a disruptive event such as an earthquake or flood. Another advantage of retrofitting is the reduction in recovery time, which in turn enhances resilience. In addition to the frameworks proposed by Bruneau et al. [15] and Cimellaro et al. [16], which defined resilience as the area under the functionality curve, Nasrazadani and Mahsuli [14] introduced a new framework for assessing community resilience based on potential costs. They proposed a novel concept of resilience for communities that allows for incorporating uncertainties and interdependencies among different infrastructures within this framework. In their study, by integrating probabilistic risk analysis models with agent-based simulation, they quantified the resilience of a hypothetical community in Tehran. Ashrafifar and Estekanchi [24] proposed an approach for rapid life-cycle resilience analysis of aging bridges using the endurance time method. In a study by Ashrafifar et al. [25], the endurance time method was employed to assess the seismic resilience of aging RC bridges subjected to seismic sequences.

Bruneau et al. [15] demonstrated that resilience is characterized by four properties: rapidity, redundancy, robustness, and resourcefulness:

1. Rapidity: the capacity to establish priorities and achieve intended goals within a time-dependent process, thereby preventing future disruptions and their adverse impacts. In this context, the slope of the functionality curve during the recovery period is considered as the measure of rapidity.
2. Robustness: refers to the strength or ability of components, systems, and other units of analysis to withstand imposed demands at a certain level without loss or degradation of functionality.
3. Redundancy: denotes the ability to substitute elements and systems that can be activated after seismic disruptions.
4. Resourcefulness: the capacity to mobilize and effectively use materials and human resources to achieve intended objectives during disruptive events.

Among these properties, rapidity and robustness are considered the primary goals for enhancing resilience, while resourcefulness and redundancy serve as the means to achieve these goals.

This study probabilistically assesses the seismic resilience of steel structures incorporating dissipative replaceable components, designed to enhance repairability and enable rapid post-earthquake recovery. The influence of these devices on fragility and vulnerability is also examined. Two steel buildings, a 6-story and a 12-story structure, are analyzed under conventional moment-resisting frames and frames with dissipative replaceable links, using detailed nonlinear models developed in OpenSees. The remainder of this paper is organized as follows: Section 2 explains the methodology for developing fragility and vulnerability curves, as well as seismic resilience assessment procedure. Section 3 presents the structural models, including the design of the steel frames and the modeling approach. Section 4 describes the selection of ground motions. Section 5 presents the results, including comparisons between conventional and link-equipped frames. Finally, Section 6 summarizes the key findings and discusses conclusions.

## 2 Methodology

### 2.1 Seismic fragility models

To evaluate the resilience and obtain recovery curves for the target structure, it is essential to first conduct an Incre-

mental Dynamic Analysis (IDA) and subsequently derive the fragility functions. IDA [26] is the most widely used method for assessing the vulnerability and fragility of building structures. In this approach, a set of earthquake records is selected, and these records are scaled at varying intensity levels (from very low to the point of structural collapse) and applied to the structure of interest. For each seismic intensity, a corresponding set of engineering demand parameters (EDPs) is obtained for each record. Finally, the results are summed up in IDA plots (or curves), which represent the engineering EDP versus intensity measure (IM) of ground motions. A careful selection of the IM plays a key role in minimizing the inherent uncertainties in probabilistic seismic demand models. By reducing these uncertainties, the accuracy of predictions concerning the performance of structures during seismic events is improved [27]. In this study, $S_a(T_1)$ is selected as an appropriate IM. For EDP, the peak inter-story drift ratio is adopted as the primary measure, since it effectively reflects the overall structural response.

IDA technique offers high accuracy by evaluating the structure's performance across a broad range of intensities, including low levels and up to collapse. However, it comes with significant computational costs. Additionally, careful consideration is required when selecting and scaling the earthquake records. For instance, scaling records with excessively large or small factors is unreasonable, as the characteristics of low-intensity records are markedly different from those of high-intensity records [28, 29].

Fragility curves are crucial tools in earthquake engineering, commonly used to evaluate the vulnerability of structures or systems under various load conditions, particularly seismic forces [30–32]. These curves provide valuable insights into the probability of specific damage levels, occurring as a function of the intensity of an external force, such as ground acceleration during an earthquake. In simpler terms, fragility curves visually depict the relationship between the intensity of a seismic event (e.g., peak ground acceleration or displacement) and the likelihood of a particular level of failure or damage. The horizontal axis of these curves typically represents the intensity of the earthquake, while the vertical axis shows the probability of exceeding a specific damage state. A typical representation of fragility functions is through lognormal cumulative distribution functions, formulated as follows [33]:

$$P\left[DS \geq DS_i \mid IM = x\right] = \left(\frac{\ln\left(\frac{x}{\theta}\right)}{\beta}\right), \tag{1}$$

where $P\left[DS \geq DS_i \mid IM = x\right]$ denotes the probability that the damage state $DS_i$ is exceeded given a ground motion with intensity measure $IM = x$. The parameters $\theta$ and $\beta$ correspond to the median and dispersion of the fragility function, respectively, while $\Phi$ represents the standard normal cumulative. Estimating $\theta$ and $\beta$, as fragility parameters, is a statistical effort. There are several statistical methods for estimating parameters based on observed data. The application of each of these techniques is dependent on the type of dynamic analysis employed to derive structural data [33]. In this study, the maximum likelihood method is utilized for estimating $\theta$ and $\beta$ as follows [33]:

$$\begin{aligned}\{\theta,\beta\} = \arg\max_{\theta,\beta} \sum_{i=1}^{m} \left\{ \ln\left( \frac{\ln\left(\frac{IM_i}{\theta}\right)}{\beta} \right) \right\} \\ + (n-m) \ln\left( 1 - \left( \frac{\ln\left(\frac{IM_{\max}}{\theta}\right)}{\beta} \right) \right),\end{aligned} \tag{2}$$

in which $n$ represents the total number of records considered, while $IM_i$ denotes the intensity measure at which the $i$-th record exceeds the specified damage threshold. The parameter $m$ corresponds to the number of records that reached this threshold, and $IM_{\max}$ indicates the maximum intensity level to which the records are scaled.

In the current study, the exceedance of damage states is defined according to the provisions of EN 1998-3:2005 standard [34], based on the plastic hinge rotations. Rotation thresholds for the RBS sections of the DRLF frame and beam ends in the reference frame are presented in Table 1.

### 2.2 Seismic vulnerability curves

Seismic vulnerability curves serve as crucial tools for evaluating potential earthquake-induced damage to structures. They enable the prediction of damage levels for different seismic intensities, and by combining the damage probabilities with the replacement (or construction) costs, direct losses can be estimated for various scenarios. Additionally, these curves are essential for assessing the seismic resilience of the system, which will be addressed later in this paper. To evaluate vulnerability, fragility

**Table 1** Damage state thresholds for fragility functions

| Frame | Damage states | | |
|---|---|---|---|
| | Minor | Moderate | Extensive |
| DRLF frame | 0.010 | 0.025 | 0.040 |
| Reference frame | 1.0 $\theta_y$ | 6.0 $\theta_y$ | 8.0 $\theta_y$ |

probabilities are transformed into loss equivalents [35]. The vulnerability of each frame under the ground motion set is then assessed by estimating its loss ratio, defined as the loss divided by the replacement cost, as follows [36]:

$$\vee[IM=x]=\sum_{k}P(DS=k\mid IM=x)\times r_k, \tag{3}$$

where $\vee[IM=x]$ denotes the loss ratio, and $P(DS=k\mid IM=x)$ represents the probability of being in the $k$-th damage state at $IM=x$. $r_k$ is the damage ratio for each damage state, calculated as the repair cost divided by the replacement cost. According to the Hazus [36], $r_k$ is 0.1, 0.25, and 0.75 for the minor, moderate, and extensive damage states, respectively. The probability of a structure being in a specific damage state can be derived from the exceedance probability of that damage state, as shown below and also illustrated in Fig. 1:

$$\begin{aligned}&P(DS=\text{Minor})\\&=P(DS\geq\text{Minor})-P(DS\geq\text{Moderate})\\&P(DS=\text{Moderate})\\&=P(DS\geq\text{Moderate})-P(DS\geq\text{Extensive})\\&P(DS=\text{Extensive})=P(DS\geq\text{Extensive})\end{aligned}. \tag{4}$$

### 2.3 Seismic resilience assessment

Resilience can be quantified through a function that reflects a system's capacity to sustain its performance over time. Fig. 2 [13] illustrates an example of such a function for a system exposed to a disruptive event. The system may represent a building, infrastructure, lifeline, or an entire city. In this study, the focus is on the resilience of DRLF frames as an effective solution for mitigating seismic damage by concentrating it in replaceable components.

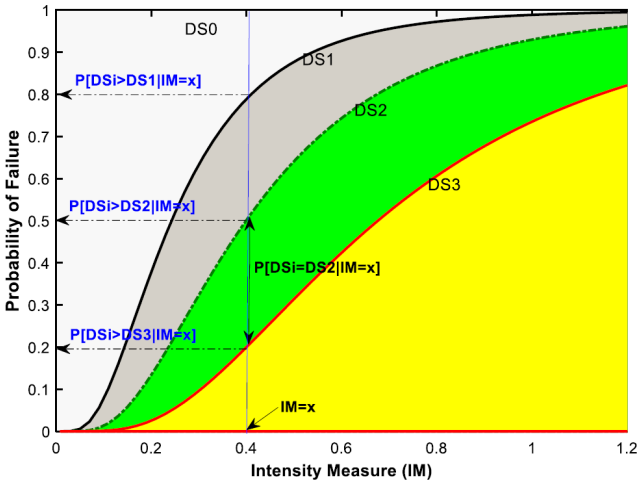


**Fig. 1** A schematic illustration of the probability of being in each damage state

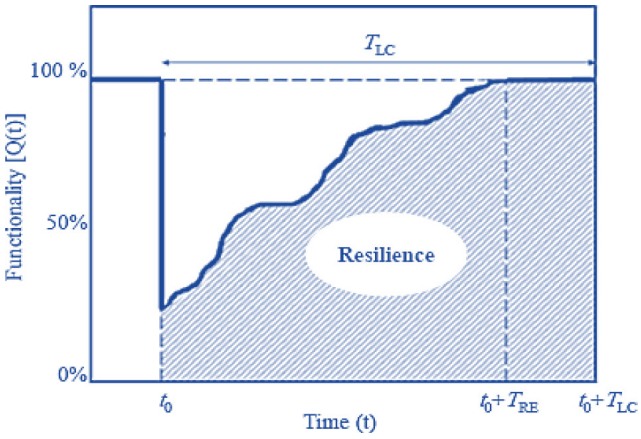


**Fig. 2** Schematic illustration of the resilience concept [13]

The framework for analytically assessing the system resilience index is expressed as follows [13, 20]:

$$R=\int_{t_{0E}}^{t_{0E}+T_{RE}}\frac{Q(t)}{T_{RE}}\times dt, \tag{5}$$

where $Q(t)$ represents the system performance or functionality (as a percentage), $t_{0E}$ is the time of the disruptive event (here seismic event), and $T_{RE}$ is the recovery time when the system regains full functionality (although the final performance may differ from the initial state). This relation essentially represents the area under the performance curve in Fig. 2. This metric can be used as a comprehensive decision variable for evaluating the performance of structures. For a structure subjected to a particular seismic event, the recovery time, $T_{RE}$, is influenced by factors including the earthquake intensity, the level of damage sustained, the effectiveness of management, and the availability of resources. The presence of numerous uncertainties in estimating $T_{RE}$ makes this the most complex aspect of resilience assessment. When no damage occurs or recovery is immediate, $Q(t)$ takes a value of 1. Conversely, in the case of complete failure with no recovery, both $Q(t)$ and the resilience index reduce to zero. Accordingly, the resilience index varies within the range of 0 to 1. The functionality function, $Q(t)$, can be expressed as:

$$Q(t)=\sum_{k=1}^{3}Q_k(t)\times P_{dmg,k}+P_{\text{undmg}}, \tag{6}$$

in which:

$$P_{dmg,k}=\begin{cases}P_{f,k}-P_{f,k+1} & 1\leq k\leq 2\\ P_{f,k} & k=3\end{cases}, \tag{7}$$

where $Q_k(t)$ represents the functionality of the frames in the $k$-th damage state, $P_{dmg,k}$ denotes the probability of being in a specific damage state, $P_{\text{undmg}}$ corresponds to the

probability of remaining undamaged, and $P_{f,k}$ indicates the probability of failure at the $k$-th damage state.

### 2.3.1 Probabilistic recovery models

A critical and challenging aspect of resilience analysis is the accurate prediction of a suitable recovery function for the structure or infrastructure in question. This element fundamentally distinguishes resilience analysis from conventional risk assessment. While risk analysis primarily aims to quantify the damage a structure may experience during a hazard and identify mitigation strategies, resilience analysis additionally requires evaluating how the structure or system restores its pre-event (or target) performance. Simulating the recovery process with precision remains a key challenge due to its inherent complexity. Various recovery functions have been proposed in the literature to model infrastructure restoration, including stepwise, linear, exponential, and trigonometric forms, among others.

When simulating the resilience of individual structures, such as buildings, simpler models can be used that incorporate uncertainties in the parameters of the recovery functions. This approach allows for more efficient modeling while reducing analytical complexity. In this regard, Cimellaro et al. [20] proposed three types of recovery functions: linear, power, and trigonometric models. The power model is applied when repairs and recovery are expected to occur rapidly, as it effectively captures a fast restoration rate. Conversely, the trigonometric model is suitable for scenarios where recovery begins slowly and accelerates over time, reflecting gradual yet increasingly rapid changes in the restoration process. The linear model is used when detailed information about the system's recovery behavior is unavailable; by assuming a constant recovery rate, it provides a simple approximation of the restoration process. In recent years, Pang and Wang [37] developed a probabilistic extension of the aforementioned framework, incorporating uncertainties associated with recovery time and the parameters governing the recovery function, thereby enabling a more precise and realistic assessment of system resilience.

Following the occurrence of an extreme event at time $t_{0E}$, an idle period $\delta_i$ is typically required before the recovery process can start at time $t_i$. The subsequent restoration phase spans a duration $\delta_r$, after which the system attains the target functionality $Q_t$ at the recovery completion time $t_r$. Accordingly, the generic functionality of the system at a given damage state, $Q_k(t)$, can be generally formulated as follows in Eq. (8) [38]:

$$Q_k(t) = Q_{r,k} + H(t - t_0 - \delta_i) \times R_{f,k}\left(\frac{t - t_0 - \delta_i}{\delta_r}\right) \times (Q_t - Q_{r,k}). \tag{8}$$

In the present study, probabilistic functions are employed using Latin Hypercube Sampling (LHS) [39] technique to illustrate the resilience behavior of steel structures equipped with energy-dissipating replaceable links and to determine the resilience index under different seismic intensities. LHS is a form of stratified Monte Carlo simulation. In this method, the cumulative distribution function is divided into $N$ equally probable intervals, and a random sample is selected from each interval. By stratifying the input probability distribution, LHS guarantees that the entire range of the distribution is sampled, leading to more accurate results even when the number of samples is limited [40]. Regarding the recovery functions, when the system experiences minor damage, it is assumed to recover rapidly to its pre-event state, typically modeled using an exponential function with zero initial delay. For moderate damage, the recovery process begins slowly and accelerates over time, making sinusoidal functions suitable for representing this behavior. In cases of severe damage or collapse, the system exhibits minimal improvement initially, with recovery accelerating only in the later stages; in this case, an exponential function with a positive coefficient is used. For a clear understanding of the recovery function considered for each damage state, refer to Fig. 3 [37]; the exact formulations of these functions are provided in Table 2 [22, 37, 38].

## 3 Description of structural models

### 3.1 Structural design of case studies

In this study, two case studies consisting of 6- and 12-story buildings are investigated. Both buildings have an

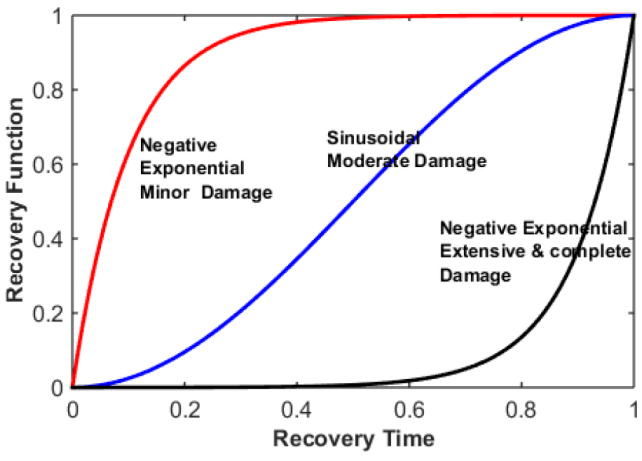


**Fig. 3** Recovery models considered in the current paper [37]

**Table 2** Recovery functions used for different damage states [22, 37, 38]

| Damage state | Type | Equation |
|---|---|---|
| Minor | Negative exponential | $1-e^{-wt}$ |
| Moderate | Sinusoidal | $\frac{1-\cos(\pi t)}{2}$ |
| Extensive | Positive exponential | $e^{-w(1-t)}$ |

inter-story height of 3.0 m and a span length of 4.275 m, and all supports are assumed as fixed supports. The structural designs follow the provisions of Section 10 of the Iranian National Building Code (INBC) [41]. Seismic and gravity loads are determined according to the Iranian Code of Practice for Seismic Resistant Design of Buildings [42] and Section 6 of the INBC [43], respectively. It is worth noting that INBC Sections 6 and 10 are largely consistent with ASCE 7-10 standard [44] and ANSI/AISC 360-10 standard [45], respectively, while Standard-2800 standard [42] is identical to ANSI/AISC 341-10 standard [46]. Structures are assumed to be residential buildings located in a highly seismic region of Tehran. The foundation soil is classified as Type 2 according to the Iranian seismic code, corresponding to an average shear wave velocity of less than 550 m/s within the depth of 30 m. The applied gravity loads include a uniform dead load of 500 kg/m$^2$ and a live load of 250 kg/m$^2$ on the floors, whereas the roof is subjected to a dead load of 550 kg/m$^2$ and a live load of 150 kg/m$^2$. The frame design accounts for the strong-column weak-beam criterion, which governs the sequence in which plastic hinges develop. The two models incorporated bracing systems to counteract longitudinal horizontal forces. The response spectrum analysis procedure is employed to design structures using the design spectrum specified in Standard-2800 standard [42]. Fig. 4 presents a 3D view of buildings equipped with replaceable energy-dissipating devices, and the structural elements for 6- and 12-story buildings are listed in Tables 3 and 4, respective.

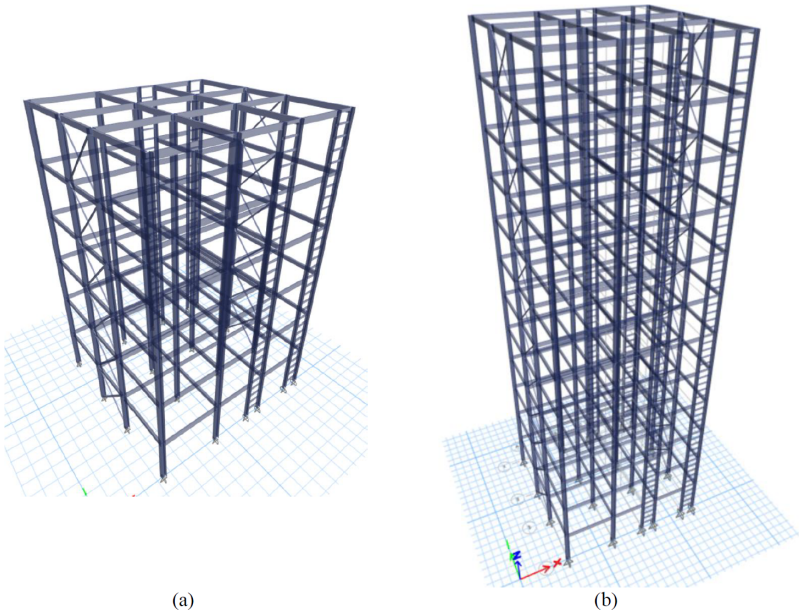

(a) (b)

**Fig. 4** 3D view of case studies equipped with replaceable energy-dissipating devices: (a) 6-story building; (b) 12-story building

**Table 3** Structural elements for 6-story building

| Floor | Pin diameter (mm) | Column section | Beam section | Brace section |
|---|---|---|---|---|
| Floors 1–2 | 45 | HEA340 | IPE300 | HEA140 |
| Floors 3–4 | 40 | HEA280 | IPE300 | HEA120 |
| Floor 5 | 35 | HEA280 | IPE300 | HEA120 |
| Floor 6 | 35 | HEA260 | IPE300 | HEA100 |

**Table 4** Structural elements for 12-story building

| Floor | Pin diameter (mm) | Column section | Beam section | Brace section |
|---|---|---|---|---|
| Floors 1–3 | 45 | HEA500 | IPE400 | HEA200 |
| Floors 3–7 | 40 | HEA450 | IPE300 | HEA160 |
| Floor 8–10 | 35 | HEA360 | IPE300 | HEA140 |
| Floor 10–12 | 35 | HEA340 | IPE300 | HEA120 |

### 3.2 Numerical models

Following the analysis and design of the studied structures, which comprise a lateral load-resisting system with moment frames and replaceable elements, the structures were subsequently modeled in the open-source structural software OpenSees [47] to perform nonlinear seismic analyses. For the reference frame (frame without replaceable energy-dissipating elements), the distributed plasticity approach is employed for beams and columns through the use of displacement-based elements with fiber sections. This approach was preferred to concentrated plasticity models as it more accurately represents the elements' behavior and accounts for the moment–axial load interaction [1]. Moreover, *Steel02* material model is used to represent the stress–strain behavior of steel elements. The overview of the numerical modeling of reference frame is represented in Fig. 5. Rayleigh damping is assigned to the first and third modes mode of the elastic response that cumulatively account for more than 95% of the total seismic mass of all frames, with a 5% damping ratio, as recommended in Chopra [48] for bolted steel structures.

In the OpenSees [47] model employed to perform IDA on the dissipative replaceable link frame, beams and braces were modeled as elastic elements because neither plasticity nor buckling occurred [1]. The beams, being irreplaceable components, were protected from yielding by the dissipative devices. The braces were designed as robust tubular sections, avoiding both buckling and yielding for seismic demands up to an average $S_a(T_1)$ of 2 g. In contrast, fiber elements were used for the columns to capture plastic behavior, specifically to identify column-base yielding. For the reduced beam sections (RBSs) of the beam links, a lumped plasticity approach is applied, concentrating material nonlinearity at specific locations. In the OpenSees [47] these parts are modeled using "*twoNodeLink*" elements. The Modified Ibarra-Krawinkler deterioration model with bilinear hysteretic response model [49, 50] is employed in the finite element software to replicate the nonlinear hysteretic behavior. The plastic rotation of the RBS, $\theta_{pl,\mathrm{RBS}}$, is determined using the formula proposed by Dougka et al. [51] (Eq. (9)), while the plastic moment, $M_{pl,\mathrm{RBS}}$, is computed in accordance with INBC-06 standard [43] (Eq. (10)):

$$\theta_{pl,\mathrm{RBS}} = \frac{W_{pl,\mathrm{RBS}} f_y L_{\mathrm{RBS}}}{6EI_{\mathrm{RBS}}}, \tag{9}$$

$$M_{pl,\mathrm{RBS}} = W_{pl,\mathrm{RBS}} f_y. \tag{10}$$

In Eqs. (9) and (10), $W_{pl,\mathrm{RBS}}$ denotes the plastic section modulus of the RBS, $f_y$ is the yield strength, $L_{\mathrm{RBS}}$ is the plastic hinge length, $E$ represents the elastic modulus of steel, and $I_{\mathrm{RBS}}$ is the moment of inertia of the RBS. The parameters defining the monotonic behavior can be analytically derived from the mechanical properties of the RBSs, in accordance

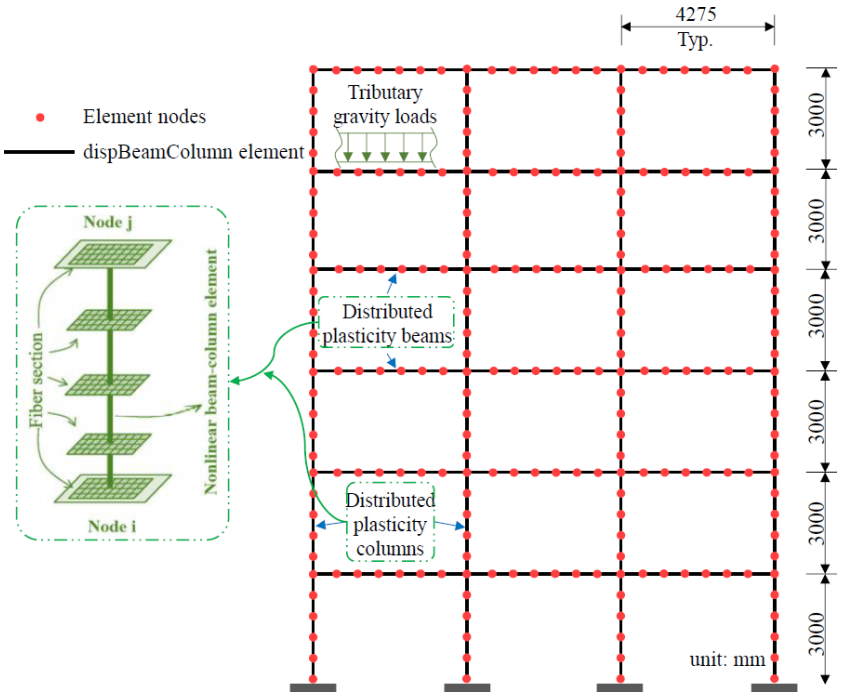


**Fig. 5** Idealized model of the reference frame

with the INNOSEIS guidelines [52]. Fig. 6 shows the numerical model of steel moment frames equipped with dissipative replaceable elements in OpenSees.

## 4 Ground motion dataset

In this study, ground motion records were not selected through a site-specific probabilistic seismic hazard analysis; rather, a generalized set of ground motions consistent with target spectra was utilized. Accordingly, 22 real far-field records from FEMA P695 report [53] are selected. The characteristics of the ground motions are provided in Table 5. The selected ground motion set consists of rare strong-motion records from high-magnitude earthquakes ($M \geq 6.5$), suitable for the site conditions of the case studies. These records cover a wide range of frequency content, intensity, and duration to capture the variability of seismic sources. In line with FEMA P695 report [53], no more than two records were taken from any single earthquake to avoid event-based bias. Consequently, the set adequately represents both record-to-record and event-to-event variability. Between the two horizontal components, the one with the higher PGA was applied to the structures.

## 5 Results and discussions

### 5.1 Seismic performance results

In Section 5.1, to provide an overall view of inter-story displacements under the design earthquake, the 22 ground motion from Section 4 are scaled to the design spectrum and applied to the structures in two configurations: with and without dissipative replaceable link. Fig. 7 compares the mean inter-story drift profiles for the DRLF and reference models. As seen, the incorporation of dissipative replaceable elements allows a significant portion of the earthquake-induced energy to be dissipated within these components. This mechanism reduces the demand on primary structural members such as beams and columns, thereby limiting their damage. As a result, the overall seismic response of the structure is improved, with noticeable reductions in inter-story drifts and enhanced protection of the main load-bearing system. This not only increases the resilience of the structure but also facilitates post-earthquake repair by confining damage to easily replaceable components.

### 5.2 Seismic fragility estimates

A comparison of the fragility curves for the two types of structures across various damage states (Fig. 8) reveals that the reference structure consistently exhibits higher fragility values. In other words, for a given seismic intensity, the probability of exceeding a specific damage state is significantly reduced when energy-dissipating links are implemented. This outcome highlights the beneficial role of the links in enhancing the probabilistic seismic performance of the structure by mitigating damage progression and improving reliability under earthquake loading. Moreover, such improvements directly contribute to

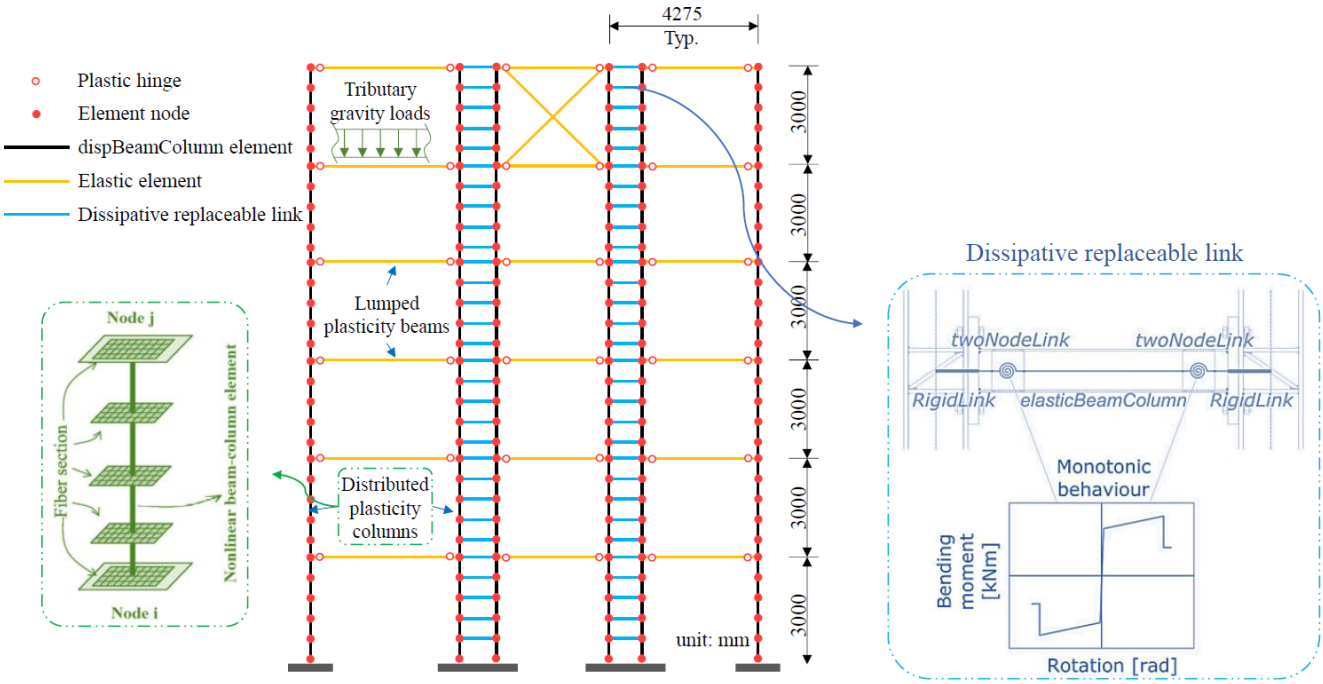


**Fig. 6** Idealized model of the dissipative replaceable link frame

**Table 5** Ground motion characteristics

| # | Event | Station | Year | *M* | PGA (dir-1) (g) | PGA (dir-2) (g) |
|---|---|---|---|---|---|---|
| 1 | Northridge | Beverly Hills-Mulholl | 1994 | 6.7 | 0.416 | 0.516 |
| 2 | Northridge | Canyon Country-WLC | 1994 | 6.7 | 0.416 | 0.482 |
| 3 | Duzce, Turkey | Bolu | 1999 | 7.1 | 0.728 | 0.822 |
| 4 | Hector Mine | Hector | 1999 | 7.1 | 0.266 | 0.337 |
| 5 | Imperial Valley | Delta | 1979 | 6.5 | 0.238 | 0.351 |
| 6 | Imperial Valley | El Centro Array #11 | 1979 | 6.5 | 0.364 | 0.380 |
| 7 | Kobe, Japan | Nishi-Akashi | 1995 | 6.9 | 0.509 | 0.503 |
| 8 | Kobe, Japan | Shin-Osaka | 1995 | 6.9 | 0.243 | 0.212 |
| 9 | Kocaeli, Turkey | Duzce | 1999 | 7.5 | 0.312 | 0.358 |
| 10 | Kocaeli, Turkey | Arcelik | 1999 | 7.5 | 0.219 | 0.150 |
| 11 | Landers | Yermo Fire Station | 1992 | 7.3 | 0.245 | 0.152 |
| 12 | Landers | Coolwater | 1992 | 7.3 | 0.283 | 0.417 |
| 13 | Loma Prieta | Capitola | 1989 | 6.9 | 0.529 | 0.443 |
| 14 | Loma Prieta | Gilroy Array #3 | 1989 | 6.9 | 0.551 | 0.367 |
| 15 | Manjil, Iran | Abbar | 1990 | 7.4 | 0.515 | 0.496 |
| 16 | Superstition Hills | El Centro Imp. Co. | 1987 | 6.5 | 0.358 | 0.258 |
| 17 | Superstition Hills | Poe Road (temp) | 1987 | 6.5 | 0.446 | 0.300 |
| 18 | Cape Mendocino | Rio Dell Overpass | 1992 | 7.0 | 0.385 | 0.549 |
| 19 | Chi-Chi, Taiwan | CHY101 | 1999 | 7.6 | 0.353 | 0.440 |
| 20 | Chi-Chi, Taiwan | TCU045 | 1999 | 7.6 | 0.474 | 0.512 |
| 21 | San Fernando | LA - Hollywood Stor | 1971 | 6.6 | 0.210 | 0.174 |
| 22 | Friuli, Italy | Tolmezzo | 1976 | 6.5 | 0.351 | 0.315 |

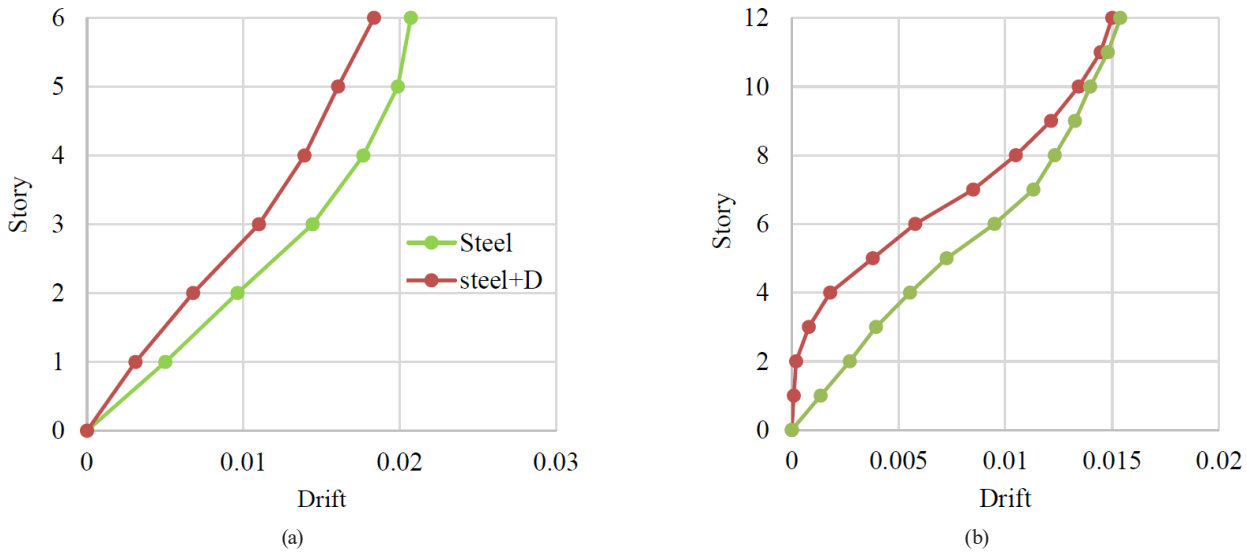


(a) (b)

**Fig. 7** Comparison of inter-story drifts for the steel structure equipped with dissipative replaceable link (Steel+D) and the reference steel structure (Steel): (a) 6-story; (b) 12-story

greater structural resilience, as they reduce the likelihood of severe damage and facilitate post-earthquake recovery by confining inelastic demands to replaceable components.

To enable comparison of the median fragility values, the IM correspond to 50% probability of failure is extracted from the curves presented above, and the results are given in Table 6. In all damage states, the reference structure (medium-ductility moment frame) exhibits higher median failure intensities than the DLRF structure. In addition, the dispersion of fragility functions is also examined. The DLRF structure demonstrated lower dispersion compared to the medium-ductility moment frame, suggesting

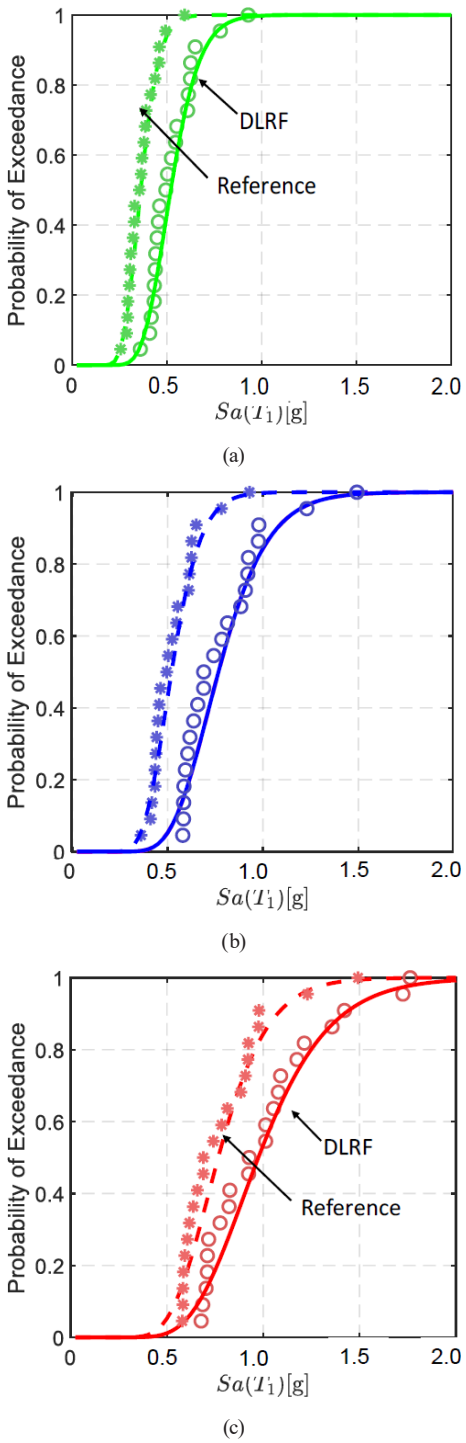


**Fig. 8** Comparison of fragility curves for the steel structure equipped with dissipative replaceable link and the reference steel structure: (a) minor damage state; (b) moderate damage state; (c) extensive damage state

**Table 6** Fragility parameters for the reference and DRLF models

| Damage states | DRLF model | | Reference model | |
|---|---|---|---|---|
| | $\theta$ | $\beta$ | $\theta$ | $\beta$ |
| Minor damage ($DS_1$) | 0.52 | 0.23 | 0.35 | 0.22 |
| Moderate damage ($DS_2$) | 0.75 | 0.26 | 0.53 | 0.23 |
| Extensive damage ($DS_3$) | 0.97 | 0.29 | 0.78 | 0.26 |

a more predictable seismic performance. This outcome is consistent with the design philosophy of using energy-dissipating links, which are intended to localize damage within predetermined replaceable components. Such a controlled damage mechanism allows for post-earthquake repair, a feature not available in conventional frames. Consequently, the reduced $\beta$ values observed in the fragility analysis confirm the improved predictability and resilience of the enhanced system.

### 5.3 Seismic vulnerability results

According to the methodology described in Section 2.2, a vulnerability curve is illustrated in Fig. 9. Fig. 9 presents the loss ratio variations for the moment-resisting frame and the system with energy-dissipating replaceable links (DLRF) as seismic intensity increases. At low intensity levels or small deformations, both systems incur minimal damage, with the curves remaining near zero. As seismic intensity or inter-story drift grows, the loss ratio increases for both frames; however, the medium-ductility steel moment frame (red curve) consistently exhibits higher values than the DLRF system (blue curve) across all intensity levels. This demonstrates that, under comparable seismic intensity conditions, the conventional moment frame is more economically vulnerable and experiences greater damage, while the inclusion of lateral links effectively reduces cumulative losses and improves the overall seismic performance of the structure.

### 5.4 Seismic resilience results

A comparison of the seismic resilience of the examined frames is presented in Section 5.4. As discussed in Section 2.3, seismic resilience is defined as a structure's

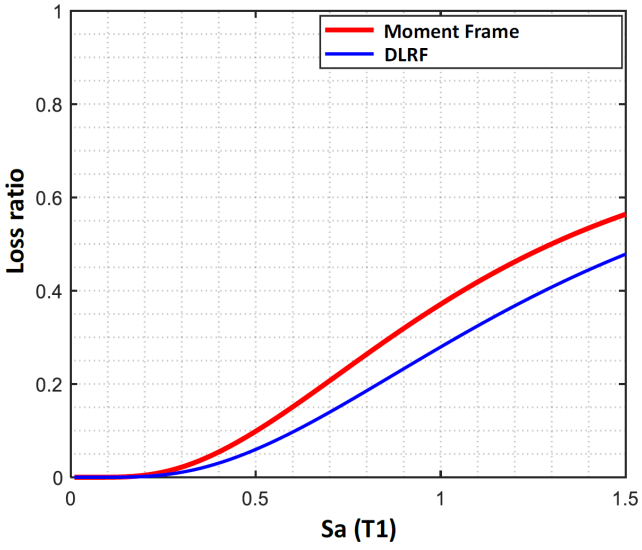


**Fig. 9** Vulnerability curves for the reference model and DLRF frame

capacity to resist earthquake forces, maintain safe operation during the event, and rapidly return to an acceptable state afterward. It involves energy absorption, limiting damage, preventing collapse, and restoring functionality within a reasonable timeframe. Beyond mere structural strength, seismic resilience also considers performance, service continuity, and the speed of recovery.

To present the results in a more intuitive manner, seismic intensity is expressed in terms of the site-specific return period, which provides a more easily understood measure. For instance, earthquakes with return periods of 475 and 2475 years are commonly cited. Developing a uniform hazard spectrum requires regional probabilistic seismic hazard data. Accordingly, the necessary information was obtained from the Iranian probabilistic seismic hazard project. In this study, the structure is assumed to be located in Tehran on type 2 soil. The hazard spectrum data for the selected site in Tehran are presented in Table 7. Using the data from Table 7, the uniform hazard spectrum for return periods of 75, 475, 975, and 2475 years is shown in Fig. 10. The recovery functions are then plotted for each seismic intensity, corresponding to return periods of 75, 475, 975, and 2475 years.

The recovery functions presented in Table 2 are employed in this study to represent damage states ranging from minor to extensive. To account for the inherent uncertainties associated with these recovery functions, a probabilistic sampling approach is applied. Specifically, 500 samples are

**Table 7** Hazard spectrum ordinates for the selected site in Tehran

| Earthquake hazard return period (year) | PGA (g) | $T = 0.2$ (s) | $T = 1.0$ (s) | $T = 3.0$ (s) |
|---|---|---|---|---|
| 75 | 0.186 | 0.450 | 0.160 | 0.041 |
| 475 | 0.390 | 0.916 | 0.375 | 0.103 |
| 975 | 0.485 | 1.149 | 0.484 | 0.132 |
| 2475 | 0.606 | 1.483 | 0.657 | 0.177 |

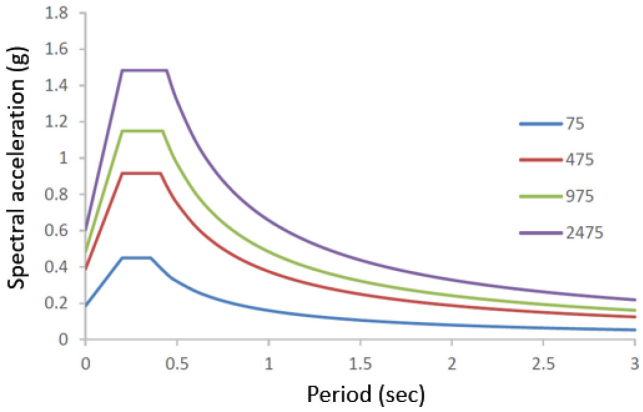


**Fig. 10** Seismic hazard spectra of the site in Tehran for different return periods

generated using LHS, ensuring a comprehensive coverage of the input parameter space. This approach allows for a more robust and realistic assessment of the structures' recovery behavior under varying levels of seismic damage, capturing both the variability in the recovery process and its impact on overall resilience. The developed recovery curves are shown in Fig. 11 for the 6-story frames and Fig. 12 for the 12-story frames. In addition, the mean recovery curve along with the corresponding standard deviations are plotted to highlight the variability in the recovery process. The area under each recovery curve corresponds to the system's resilience. Since the recovery functions are probabilistic, the mean function provides a representative value for the resilience index in the present study. Fig. 13 presents a comparison of the resilience indices for both frames. It is evident that the frame equipped with energy-dissipating links exhibits higher resilience than the conventional moment frame across all seismic scenarios. The difference is particularly significant for high-intensity events, such as the 2475-year return period earthquake, demonstrating the effectiveness of these links in enhancing performance under severe and rare seismic events.

The results depicted in Figs. 11 to 13 indicate that for short return periods (75 years) and low-intensity seismic events, there is little difference between the two frames, with both exhibiting resilience indices close to one. As the seismic intensity and return period increase to 475 and 975 years, the conventional frame shows a more pronounced decline in resilience, whereas the frame equipped with energy-dissipating links is able to maintain higher resilience values. This disparity becomes even more evident under extreme events with a 2475-year return period: the resilience index of the conventional frame decreases to approximately 0.69, while the link-equipped frame sustains a higher level of around 0.8. Consequently, incorporating energy-dissipating links significantly enhances both the resilience and the reliability of structures, particularly during rare and high-intensity earthquake events.

### 5.5 Evaluation of sample sufficiency

Section 5.5 evaluates whether the number of samples adopted for the recovery functions is statistically adequate. As mentioned, 500 samples were employed to develop the probabilistic recovery curves. To verify their sufficiency, a sensitivity analysis is conducted. For this purpose, samples are generated using different numbers of simulations, and the resilience index is calculated. As seen in Fig. 14, resilience index tends to converge to

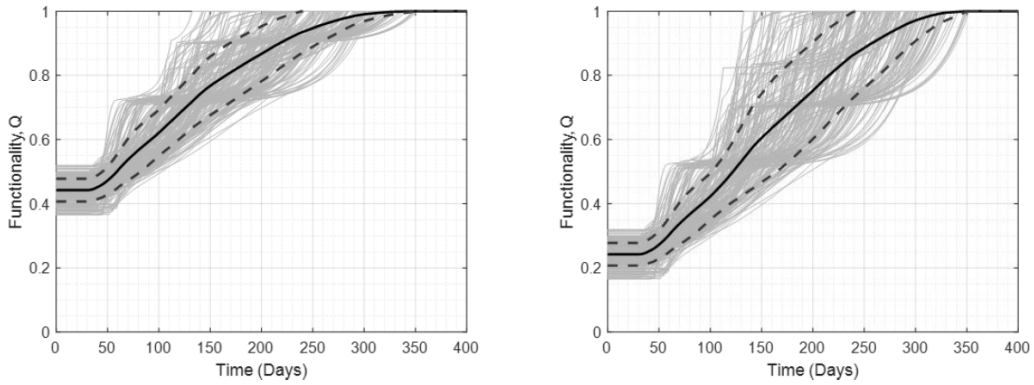


(a)

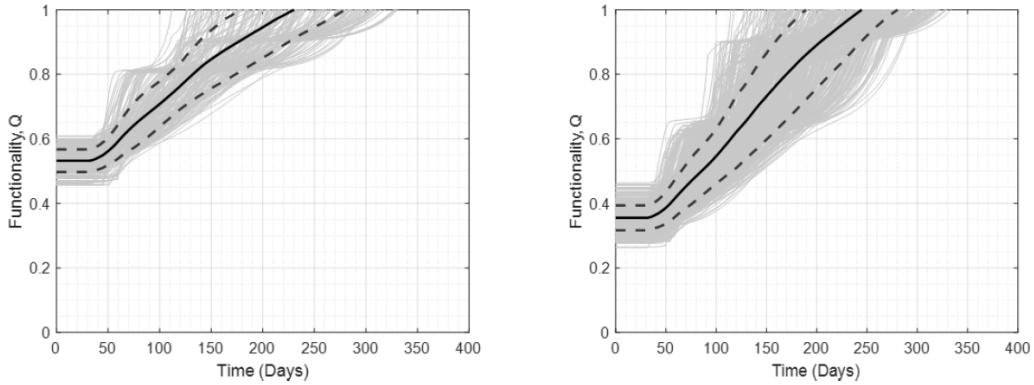


(b)

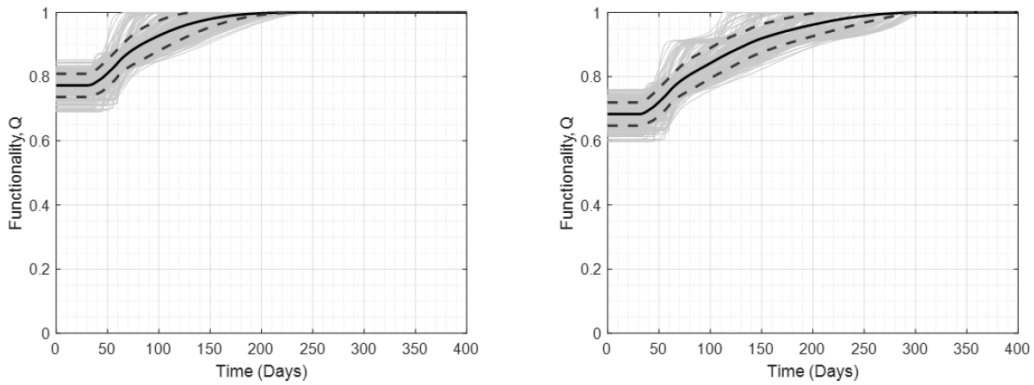


(c)

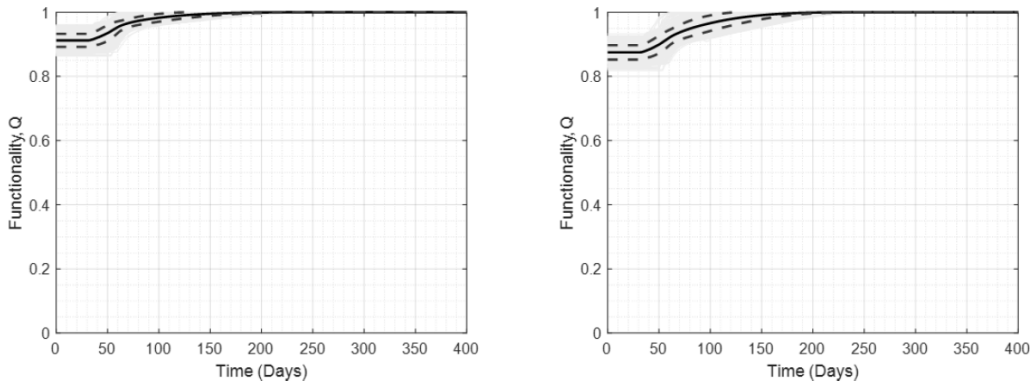


(d)

**Fig. 11** Probabilistic recovery functions for 6-story DRLF frame (left) and reference frame (right) under: (a) 2475-year; (b) 975-year; (c) 475-year; (d) 75-year seismic scenarios

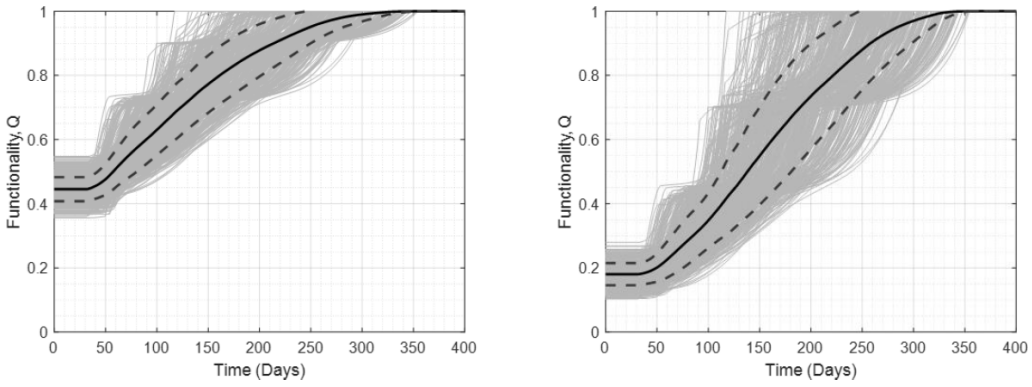


(a)

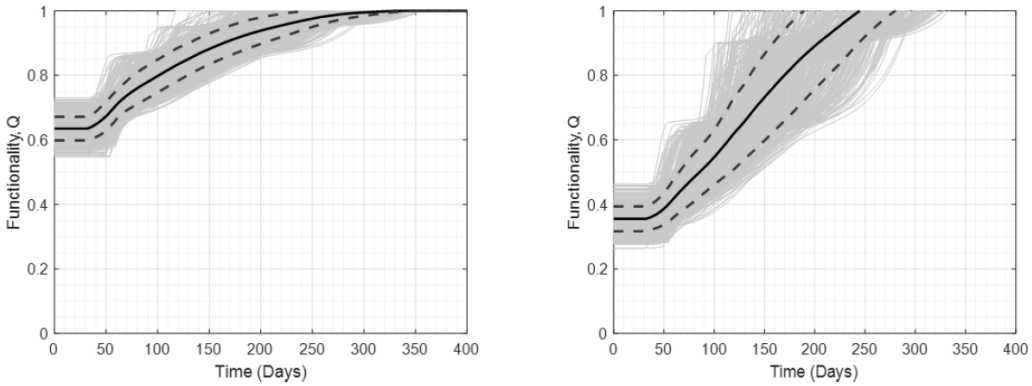


(b)

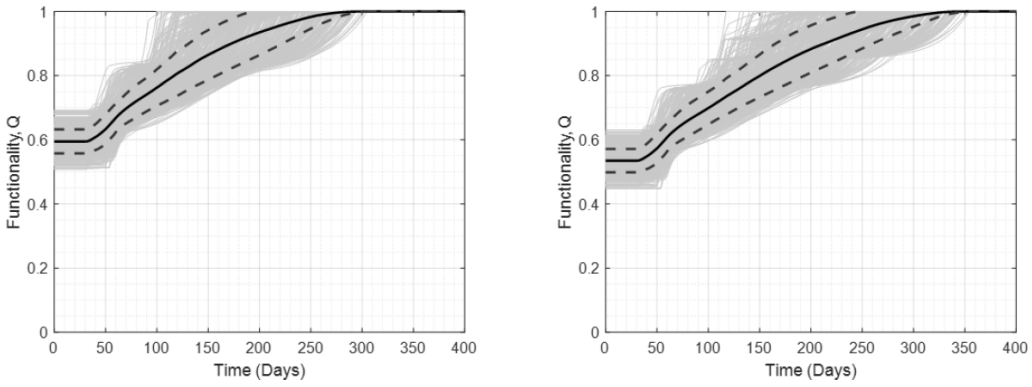


(c)

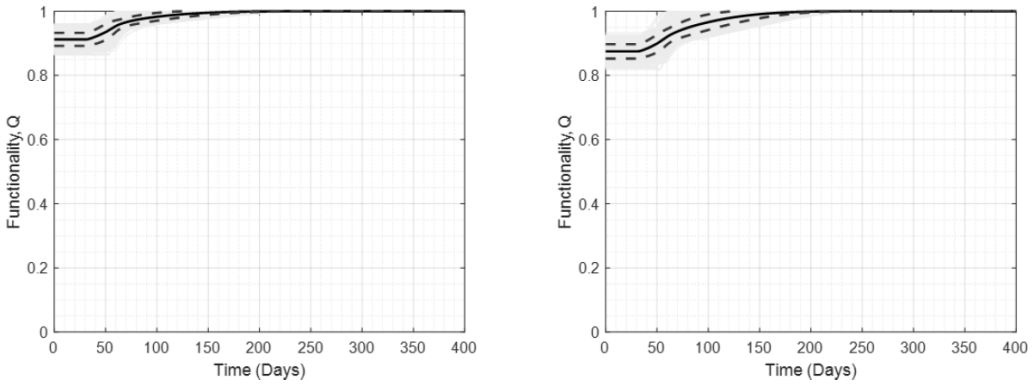


(d)

**Fig. 12** Probabilistic recovery functions for 12-story DRLF frame (left) and reference frame (right) under: (a) 2475-year; (b) 975-year; (c) 475-year; (d) 75-year seismic scenarios

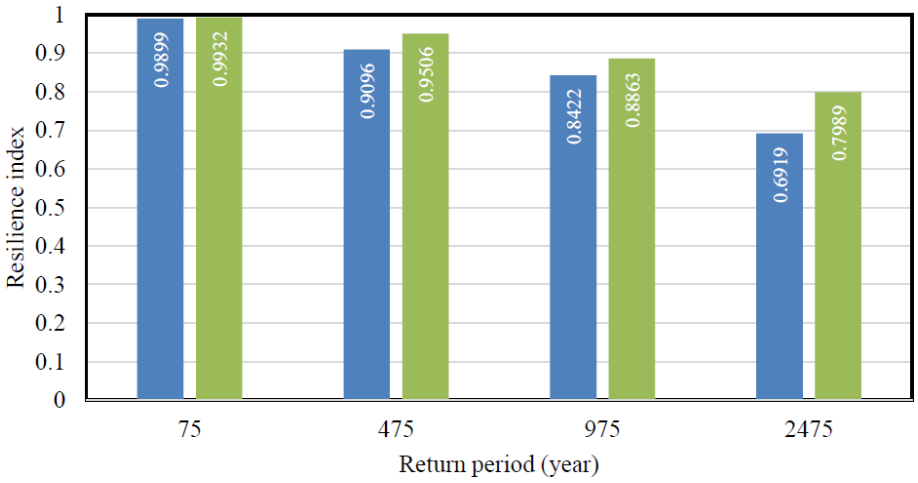


(a)

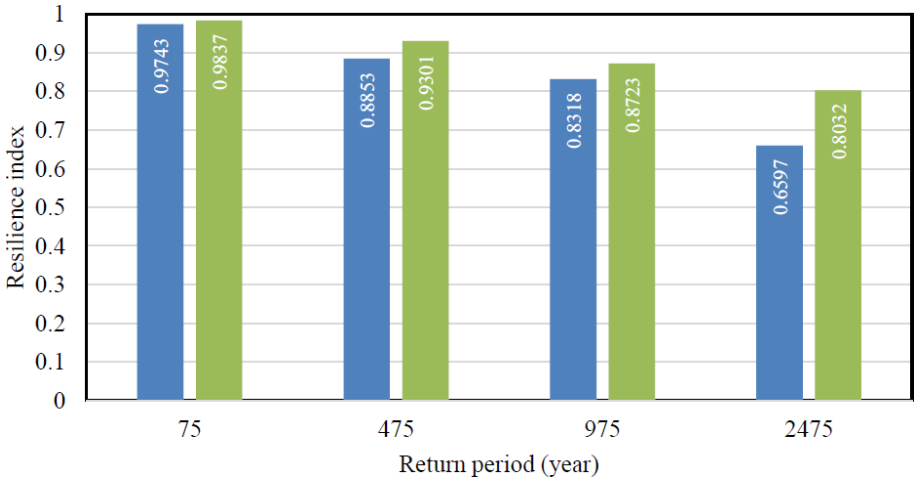


(b)

**Fig. 13** Resilience indices for: (a) 6-story and (b) 12-story DRLF frames (blue bars) and reference frames (green bars)

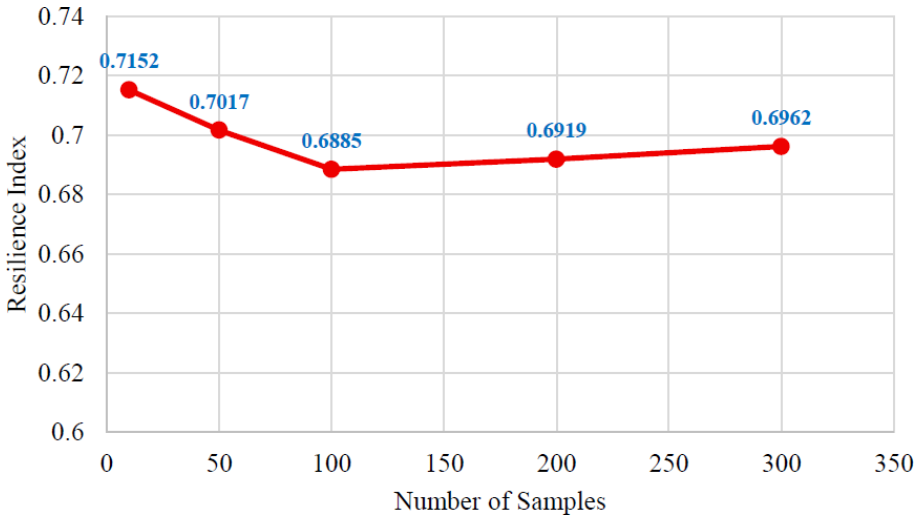


**Fig 14** Influence of the number of recovery function simulations on the resilience index

a stable value as the number of simulations increases. Beyond a certain point, the variation in results becomes negligible; specifically, after 300 samples, differences fall below 1%. Therefore, the 500 simulations conducted in this study provide a statistically sufficient basis, ensuring the reliability of the obtained results.

## 6 Conclusions

This study investigated the seismic resilience of steel moment frames equipped with energy-dissipating replaceable links, as well as their effects on fragility functions and vulnerability curves. For these purposes, this research focused on two steel structures, a 6-story and a 12-story building, analyzed under two configurations: conventional moment-resisting frames and frames incorporating energy-dissipating replaceable links. The preliminary designs were conducted and detailed nonlinear models were developed in OpenSees. IDA procedure was subsequently carried out using 22 ground motion records recommended in FEMA P695 report [52]. Based on these results, fragility curves were derived for the studied frames, providing a practical means to evaluate seismic vulnerability and resilience. The loss ratios as a function of earthquake intensity measures were obtained through vulnerability analysis. Subsequently, the seismic resilience of the conventional moment frame and the moment frame equipped with energy-dissipating links was evaluated across different return periods, in order to assess resilience under varying seismic intensity levels. The framework for resilience assessment must be probabilistic to adequately account for the uncertainties associated with recovery functions. To this end, different recovery functions were considered for each of the three damage states, with 500 samples generated for each (using LHS technique), in order to derive probabilistic resilience curves. Significant conclusions are summarized below:

- The analysis results indicate that the inter-story drift in structures equipped with dissipative devices was consistently lower across all earthquake intensity levels compared to conventional frames. This reduction in drift also helps mitigate secondary damage to non-structural components such as partition walls and facades. In conventional frames, damage was distributed unevenly and primarily concentrated in critical beam and column regions. By contrast, in frames with dissipative replaceable devices, damage was localized mainly in the replaceable links, leaving the primary members largely intact.
- The extracted fragility curves showed that the probability of reaching damage states under different earthquake intensities was significantly reduced when using dissipative replaceable devices. This improvement was particularly pronounced at performance levels corresponding to life safety and collapse prevention, where notable differences between the two types of frames were observed.
- Resilience indices further demonstrated that frames with replaceable links possess superior capacity to maintain functionality and recover more quickly after seismic events. This benefit is especially critical under strong earthquakes, where conventional frames required extensive repair (leading to lower resilience indices), while link-equipped frames could be restored to their original condition by replacing only a few localized elements.
- The assessment of 6- and 12-story buildings revealed that the positive effects of energy-dissipating links were evident at different heights. However, for some return periods, the resilience index of the 12-story link-equipped structure showed even more pronounced improvement. This finding underscores the particularly important role of dissipative links in enhancing seismic resilience and controlling structural response in taller buildings.

Overall, the findings of this study demonstrated that the use of dissipative replaceable elements is an effective and efficient strategy for enhancing the seismic performance and resilience of steel moment frames. This system not only improves safety and reduces the probability of failure but also limits overall deformations, concentrates damage in replaceable components, and reduces both the cost and time of post-earthquake recovery.

## References

[1] Giuliani, G., Andreotti, R., Tondini, N. "Probabilistic seismic demand models of steel structures equipped with dissipative replaceable devices", Journal of Constructional Steel Research, 229, 109520, 2025.
https://doi.org/10.1016/j.jcsr.2025.109520

[2] Giuliani, G., Andreotti, R., Tondini, N. "Hybrid simulation of a steel frame with Dissipative Replaceable Link Frames", Bulletin of Earthquake Engineering, 22(8), pp. 4023–4053, 2024.
https://doi.org/10.1007/s10518-024-01907-y

[3] Elqudah, S. M., Vigh, L. G. "Coexisting with Disasters: A State-of-the-art Review of Resilience Assessment of Steel Structures under Extreme Hazards", Periodica Polytechnica Civil Engineering, 69(4), pp. 1187–1202, 2025.
https://doi.org/10.3311/PPci.40641

[4] Andreotti, R., Giuliani, G., Tondini, N. "Experimental analysis of a full-scale steel frame with replaceable dissipative connections", Journal of Constructional Steel Research, 208, 108036, 2023.
https://doi.org/10.1016/j.jcsr.2023.108036

[5] Giuliani, G., Andreotti, R., Bonelli, A., Tondini, N. "Hybrid simulation of steel frames with Dissipative Replaceable Link Frame and high-strength steel coupling beams", Engineering Structures, 316, 118551, 2024. https://doi.org/10.1016/j.engstruct.2024.118551

[6] Tondini, N., Zanon, G., Pucinotti, R., Di Filippo, R., Bursi, O. S. "Seismic performance and fragility functions of a 3D steel-concrete composite structure made of high-strength steel", Engineering Structures, 174, pp. 373–383, 2018. https://doi.org/10.1016/j.engstruct.2018.07.026

[7] Latour, M., Piluso, V., Rizzano, G. "Free from damage beam-to-column joints: Testing and design of DST connections with friction pads", Engineering Structures, 85, pp. 219–233, 2015. https://doi.org/10.1016/j.engstruct.2014.12.019

[8] Latour, M., Rizzano, G., Santiago, A., Simões da Silva, L. "Experimental response of a low-yielding, self-centering, rocking column base joint with friction dampers", Soil Dynamics and Earthquake Engineering, 116, pp. 580–592, 2019. https://doi.org/10.1016/j.soildyn.2018.10.011

[9] Calado, L., Proença, J. M., Espinha, M., Castiglioni, C. A. "Hysteretic behaviour of dissipative bolted fuses for earthquake resistant steel frames", Journal of Constructional Steel Research, 85, pp. 151–162, 2013. https://doi.org/10.1016/j.jcsr.2013.02.016

[10] Elettore, E., Lettieri, A., Freddi, F., Latour, M., Rizzano, G. "Performance-based assessment of seismic-resilient steel moment resisting frames equipped with innovative column base connections", Structures, 32, pp. 1646–1664, 2021. https://doi.org/10.1016/j.istruc.2021.03.072

[11] Elettore, E., Freddi, F., Latour, M., Rizzano, G. "Design and analysis of a seismic resilient steel moment resisting frame equipped with damage-free self-centering column bases", Journal of Constructional Steel Research, 179, 106543, 2021. https://doi.org/10.1016/j.jcsr.2021.106543

[12] Kanyilmaz, A., Kondratenko, A., Castiglioni, C. A., Calado, L., Proenca, J., …, Salvatore, W. "Fully dissipative and easily repairable components for resilient buildings with composite steel-concrete structures", Eurpean Commission, Brussels, Belgium, Rep. 800699, 2022. [online] Available at: http://dissipable.ntua.gr [Accessed: 31 October 2025]

[13] Cimellaro G. P. "Urban Resilience for Emergency Response and Recovery: Fundamental Concepts and Applications", Springer Cham, 2016. ISBN 978-3-319-30656-8 https://doi.org/10.1007/978-3-319-30656-8

[14] Nasrazadani, H., Mahsuli, M. "Probabilistic Framework for Evaluating Community Resilience: Integration of Risk Models and Agent-Based Simulation", Journal of Structural Engineering, 146(11), 04020250, 2020. https://doi.org/10.1061/(ASCE)ST.1943-541X.0002810

[15] Bruneau, M., Chang, S. E., Eguchi, R. T., Lee, G. C., O'Rourke, T. D., Reinhorn, A. M., Shinozuka, M., Tierney, K., Wallace, W. A., von Winterfeldt, D. "A Framework to Quantitatively Assess and Enhance the Seismic Resilience of Communities", Earthquake Spectra, 19(4), pp. 733–752, 2003. https://doi.org/10.1193/1.1623497

[16] Cimellaro, G. P., Fumo, C., Reinhorn, A. M., Bruneau, M. "Quantification of Disaster Resilience of Health Care Facilities", MCEER: Earthquake Engineering to Extreme Events, Buffalo, NY, USA, Rep. MCEER-09-0009, 2009. [online] Available at: https://www.buffalo.edu/mceer/catalog.host.html/content/shared/www/mceer/publications/MCEER-09-0009.detail.html [Accessed: 31 October 2025]

[17] Bruneau, M., Reinhorn, A. "Exploring the Concept of Seismic Resilience for Acute Care Facilities", Earthquake Spectra, 23(1), pp. 41–62, 2007. https://doi.org/10.1193/1.2431396

[18] Wang, C., Ayyub, B. M. "Time-dependent seismic resilience of aging repairable structures considering multiple damage states", Earthquake Engineering and Resilience, 1(1), pp. 73–87, 2022. https://doi.org/10.1002/eer2.5

[19] Klein, R. J. T., Nicholls, R. J., Thomalla, F. "Resilience to natural hazards: How useful is this concept?", Global Environmental Change Part B: Environmental Hazards, 5(1), pp. 35–45, 2003. https://doi.org/10.1016/j.hazards.2004.02.001

[20] Cimellaro, G. P., Reinhorn, A. M., Bruneau, M. "Framework for analytical quantification of disaster resilience", Engineering Structures, 32(11), pp. 3639–3649, 2010. https://doi.org/10.1016/j.engstruct.2010.08.008

[21] Cimellaro, G. P., Renschler, C., Reinhorn, A. M., Arendt, L. "PEOPLES: A Framework for Evaluating Resilience", Journal of Structural Engineering, 142(10), 04016063, 2016. https://doi.org/10.1061/(ASCE)ST.1943-541X.0001514

[22] Cimellaro, G. P., Reinhorn, A. M., Bruneau, M. "Seismic resilience of a hospital system", Structure and Infrastructure Engineering, 6(1–2), pp. 127–144, 2010. https://doi.org/10.1080/15732470802663847

[23] Berman, J. W., Bruneau, M. "Experimental Investigation of Light-Gauge Steel Plate Shear Walls for the Seismic Retrofit of Buildings", Multidisciplinary Center for Earthquake Engineering Research, University of Buffalo, Buffalo, NY, USA, Rep. MCEER-03-0001, 2003. [online] Available at: https://www.eng.buffalo.edu/mceer-reports/03/03-0001.pdf [Accessed: 31 October 2025]

[24] Ashrafifar, J., Estekanchi, H. "Life-cycle seismic fragility and resilience assessment of aging bridges using the endurance time method", Soil Dynamics and Earthquake Engineering, 164, 107524, 2023. https://doi.org/10.1016/j.soildyn.2022.107524

[25] Ashrafifar, B., Javaherian, P., Ashrafifar, J. "Seismic resilience analysis of aging RC bridges subjected to seismic sequences via intensifying excitation functions", Structures, 73, 108406, 2025. https://doi.org/10.1016/j.istruc.2025.108406

[26] Vamvatsikos, D., Cornell, C. A. "Incremental dynamic analysis", Earthquake Engineering & Structural Dynamics, 31(3), pp. 491–514, 2002. https://doi.org/10.1002/eqe.141

[27] Taghizadeh, M., Delaviz, A., Akbarzadeh, M. R., Estekanchi, H. E. "Optimal seismic intensity measure selection for high voltage electrical substation equipment in various setup configurations", Soil Dynamics and Earthquake Engineering, 190, 109106, 2025. https://doi.org/10.1016/j.soildyn.2024.109106

[28] Delaviz, A., Yaghmaei-Sabegh, S., Souri, O. "Seismic Fragility and Reliability of Base-Isolated Structures with Regard to Superstructure Ductility and Isolator Displacement Considering Degrading Behavior", Journal of Earthquake Engineering, 28(14), pp. 3973–4002, 2024. https://doi.org/10.1080/13632469.2024.2360120

[29] Baker J. W. "Measuring Bias in Structural Response Caused by Ground Motion Scaling", presented at 8th Pacific Conference on Earthquake Engineering, Singapore, Singapore, Dec. 5–7., 2007.

[30] Ashrafifar, J., Hajihassani, M., Kharghani, M. "Lifetime seismic fragility assessment of subway stations using the endurance time analysis (ETA) method", Structures, 80, 109647, 2025. https://doi.org/10.1016/j.istruc.2025.109647

[31] Akbarzadeh, M. R., Delaviz, A., Zolfaghari, M., Estekanchi, H. E., Tabeshpour, M. R. "A framework for rapid seismic fragility analysis of offshore wind turbines considering wind, wave and scour", Soil Dynamics and Earthquake Engineering, 198, 109620, 2025. https://doi.org/10.1016/j.soildyn.2025.109620

[32] Liu, C., Fang, D., Yan, Z. "Seismic Fragility Analysis of Base Isolated Structure Subjected to Near-fault Ground Motions", Periodica Polytechnica Civil Engineering, 65(3), pp. 768–783, 2021. https://doi.org/10.3311/PPci.15276

[33] Baker, J. W. "Efficient Analytical Fragility Function Fitting Using Dynamic Structural Analysis", Earthquake Spectra, 31(1), pp. 579–599, 2015. https://doi.org/10.1193/021113EQS025M

[34] CEN "EN 1998-3:2005 Eurocode 8: Design of structures for earthquake resistance - Part 3: Assessment and retrofitting of buildings", European Committee of Standardization, Brussels, Belgium, 2005.

[35] Delaviz, A., Ashrafifar, J., Norouzi, N., Taghizadeh, M., Yaghmaei-Sabegh, S. "Uncertainty and bias in probabilistic seismic assessment of high voltage substation equipment under varied ground motion characteristics", Structures, 75, 108820, 2025. https://doi.org/10.1016/j.istruc.2025.108820

[36] FEMA "Hazus Earthquake Model Technical Manual (Hazus 5.1)", [pdf] Federal Emergency Management Agency, 2022. Available at: https://www.fema.gov/sites/default/files/documents/fema_hazus-earthquake-model-technical-manual-5-1.pdf [Accessed: 31 October 2025]

[37] Pang, Y., Wang, X. "Enhanced endurance-time-method (EETM) for efficient seismic fragility, risk and resilience assessment of structures", Soil Dynamics and Earthquake Engineering, 147, 106731, 2021. https://doi.org/10.1016/j.soildyn.2021.106731

[38] Biondini, F., Camnasio, E., Titi, A. "Seismic resilience of concrete structures under corrosion", Earthquake Engineering & Structural Dynamics, 44(14), pp. 2445–2466, 2015. https://doi.org/10.1002/eqe.2591

[39] Mckay, M. D., Beckman, R. J., Conover, W. J. "A Comparison of Three Methods for Selecting Values of Input Variables in the Analysis of Output From a Computer Code", Technometrics, 42(1), pp. 55–61, 2000. https://doi.org/10.1080/00401706.2000.10485979

[40] Delaviz, A., Estekanchi, H. E. "A rapid seismic fragility and risk analysis of electrical substation equipment considering modeling uncertainties", Engineering Structures, 293, 116686, 2023. https://doi.org/10.1016/j.engstruct.2023.116686

[41] INBC "INBC-10 Design and Construction of Steel Structures", Iranian National Building Code, Tehran, Iran, 2013.

[42] INBC "Standard-2800 Iranian Code of Practice for Seismic Resistant Design of Buildings", Iranian National Building Code, Tehran, Iran, 2014.

[43] INBC "INBC-06 Loading", Iranian National Building Code, Tehran, Iran, 2013.

[44] ASCE "ASCE 7-10 Minimum Design Loads for Buildings and Other Structures", American Society of Civil Engineering, Reston, VA, USA, 2010.

[45] AISC "ANSI/AISC 360-10 Specification for Structural Steel Buildings", American Institute of Steel Construction, Chicago, IL, USA, 2010.

[46] AISC "ANSI/AISC 341-10 Seismic Provisions for Structural Steel Buildings", American Institute of Steel Construction, Chicago, IL, USA, 2010.

[47] McKenna F., Fenves G., Scott M. "OpenSees: Open system for earthquake engineering simulation, (Version)", [computer program] Available at: https://opensees.berkeley.edu [Accessed: 31 October 2025]

[48] Chopra, A. K. "Dynamics of Structures: Theory and Applications to Earthquake Engineering", Pearson, 2017. ISBN 9780134555126

[49] Ibarra, L. F., Medina, R. A., Krawinkler, H. "Hysteretic models that incorporate strength and stiffness deterioration", Earthquake Engineering & Structural Dynamics, 34(12), pp. 1489–1511, 2005. https://doi.org/10.1002/eqe.495

[50] Lignos, D. G., Krawinkler, H. "Deterioration Modeling of Steel Components in Support of Collapse Prediction of Steel Moment Frames under Earthquake Loading", Journal of Structural Engineering, 137(11), pp. 1291–1302, 2011. https://doi.org/10.1061/(ASCE)ST.1943-541X.0000376

[51] Dougka, G., Dimakogianni, D., Vayas, I. "Innovative energy dissipation systems (FUSEIS 1-1) — Experimental analysis", Journal of Constructional Steel Research, 96, pp. 69–80, 2014. https://doi.org/10.1016/j.jcsr.2014.01.003

[52] Vayas I. (ed.) "Innovative Anti-Seismic Devices and Systems: Research Fund for Coal and Steel INNOSEIS Project RFCS-02-2015", ECCS – European Convention for Constructional Steelwork, 2017. ISBN 978-92-9147-136-2 [online] Available at: http://innoseis.ntua.gr [Accessed: 31 October 2025]

[53] FEMA "Quantification of Building Seismic Performance Factors", Federal Emergency Management Agency, Washington, DC, USA, Rep. FEMA P695, 2009.